Predicting instabilities of a tuneable ring laser with an iterative map model

BRADY METHERALL[1,3] **AND C. SEAN BOHUN**[2,4]

[1] *Mathematical Institute, University of Oxford, Radcliffe Observatory Quarter, Woodstock Rd, Oxford OX2 6GG, UK*
[2] *Faculty of Science, University of Ontario Institute of Technology, 2000 Simcoe St N, Oshawa, ON L1G 0C5, Canada*
[3] *brady.metherall@maths.ox.ac.uk*
[4] *sean.bohun@ontariotechu.ca*

Compiled December 3, 2020

Simple mathematical models have been unable to predict the conditions leading to instabilities in a tuneable ring laser. Here, we propose a nonlinear iterative map model for tuneable ring lasers. Solving a reduced nonlinear Schrödinger equation for each component in the laser cavity, we obtain an algebraic map for each component. Iterating through the maps gives the total effect of one round trip. By neglecting the nonlinearity initially, we find a linearly chirped Gaussian to be the analytic fixed point solution, which we analyze asymptotically. We then numerically solve the full nonlinear model, allowing us to probe the underlying interplay of dispersion, modulation, and nonlinearity, as the pulse evolves over hundreds of round trips of the cavity. In the nonlinear case, we find the chirp saturates, and the Fourier transform of the pulse becomes more rectangular in shape. Finally, for a nominal plane in the parameter space, we uncover a rich, sharp boundary separating the stable region and the unstable region where modulation instability degrades the pulse into an unsustainable state.

http://dx.doi.org/10.1364/ao.XX.XXXXXX

1. INTRODUCTION

Dispersion-tuned actively mode-locked lasers are an active area of optics research since they have a wide range of applications. These lasers can have ultrashort pulses, as short as 50 femtoseconds [1], and the ability to tune their output frequency rapidly over a range of over 100 nm [1–4]. The capability to alter the operating frequency makes tuneable lasers particularly useful for imaging applications, such as optical coherence tomography [2, 4, 5], coherent anti-Stokes Raman spectroscopy [5], and deep tissue multi-photon microscopy [1]; as well as sensing and measuring of other ultrafast processes [5–7]. Tuneable lasers are usually constructed in a ring with five main components: optical coupler, chirped fibre Bragg grating (CFBG), modulator (or saturable absorber), Er-doped fibre, and pump laser. A typical ring laser cavity is depicted in Fig. 1. The Kerr nonlinearity plays a crucial role in the dynamics within the cavity due to the high power and ultrashort duration of the pulses.

Several effects arise within the cavity due to the interplay of dispersion, modulation, and the nonlinearity [2, 7–12]. The two effects of most interest for this paper are wave breaking, and modulation instability. Wave breaking causes the leading edge of a pulse to redshift, and the trailing edge to blueshift (the effect reverses in the anomalous dispersion regime) to the point a shock develops [13–17]. The frequency shift causes the pulse to become more rectangular in the frequency domain, with a linear chirp over most of the pulse, saturating at the leading and trailing edge. In optics, wave breaking manifests from self-phase modulation (SPM), which is a direct effect of the Kerr nonlinearity, causing the pulse to interfere with itself. New frequencies are then generated such that a rectangular profile is induced [12, 18]. Modulation instability—which typically arises in the anomalous dispersion regime—is the other effect that will be of interest. However, in the presence of multiple frequencies, modulation instability can emerge in the normal dispersion regime as well through cross-phase modulation and four-wave mixing [18–20]. Modulation instability causes a pulse to degrade into much shorter, less intense pulses, and can cause a laser to lose coherence [8, 19, 20]. Outside of optics, wave breaking and modulation instability occur in other areas with nonlinear waves and dispersive media such as plasma physics, heat propagation, transmission lines, and fluid dynamics [8, 15]. Within a ring laser cavity, wave breaking and modulation instability can become parasitic leading to an unstable and unsustainable pulse. Understanding the rich landscape of the parameter space is important for determining design principles to guarantee the ring laser is stable and sustainable [2, 9, 12, 21, 22].

The canonical equation in nonlinear optics is the nonlinear Schrödinger equation,

$$\frac{\partial A}{\partial z} = -i\frac{\beta_2}{2}\frac{\partial^2 A}{\partial T^2} + i\gamma|A|^2 A. \tag{1}$$

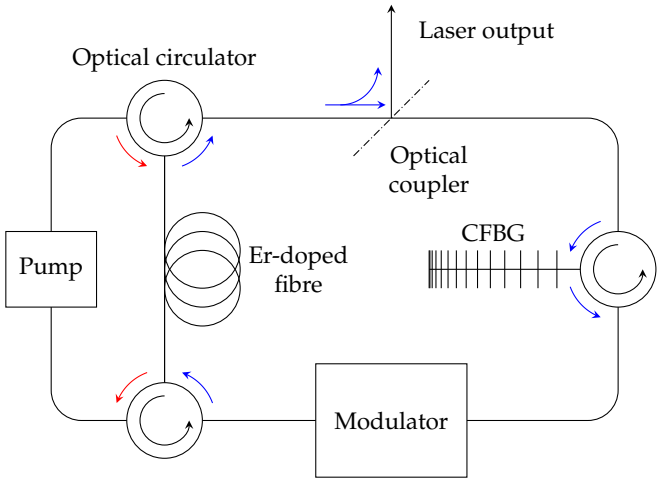

Fig. 1. Common cavity of a fibre ring laser [1, 5, 9, 11]. The pump laser travels clockwise around the left-hand loop (red arrows) energizing the Er-doped fibre. The main laser travels clockwise around the right-hand loop (blue arrows), with most of the pulse exiting the cavity through the optical coupler.

Here, $A = A(T,z)$ is the complex pulse envelope, T is co-moving time, z is the propagation coordinate, and β_2 and γ are the group velocity dispersion and Kerr nonlinearity, respectively. Typically, Eq. (1) is generalized to incorporate terms more specific to laser physics. A gain term and a loss term are added (and sometimes higher order dispersion terms), to yield the generalized nonlinear Schrödinger equation (GNLSE) [2, 18, 22–25],

$$\frac{\partial A}{\partial z} = -i\frac{\beta_2}{2}\frac{\partial^2 A}{\partial T^2} + i\gamma|A|^2A + \frac{1}{2}g(A)A - \alpha A, \tag{2}$$

where $g(A)$ is an amplifying term owing to the gain fibre, and α is the loss due to scattering and absorption.

The GNLSE, Eq. (2), has applications in nonlinear optics and fibre optic communications, however, Eq. (2) is regularly generalized even further to include a modulation term. The resulting equation is referred to as the master equation of mode-locking (see [26–30]), or sometimes the Ginzburg–Landau equation. Owing to the nonlinear term in Eq. (2) and the often non-trivial form of $g(A)$, as well as the possible addition of a modulation term, no analytic solution is known to the master equation or to Eq. (2). See Haus [28] for a comprehensive description and history of the theory of mode-locked lasers. While the GNLSE well represents the dynamics in, say, a single optical fibre, Eq. (2) is not entirely representative of the underlying physics within a laser cavity such as Fig. 1. An assumption of Eq. (2) is each process affects the pulse continuously within the cavity. Therefore, the GNLSE, and generalizations, can be thought of as an 'average' model for lasers—this assumption breaks down if the pulse undergoes large changes during any one round trip. Often, this assumption does not hold because of the specialized, discrete components.

In this paper, we will build an iterative map model for the evolution of a laser pulse as the pulse travels through the cavity. In Section 2, we will briefly review previous iterative map models, then, we will derive our own iterative map model from Eq. (2). We will then non-dimensionalize the model and introduce four dimensionless parameters that govern the dynamics of the system. We will then examine the results of our model in Section 3—first solving the model analytically by assuming the absence of the nonlinearity, then numerically solving the full nonlinear model. We will identify a sharp boundary in the parameter space separating the region of stability, and the region where modulation instability degrades the pulse. Finally, the concluding thoughts and ideas for possible future work are given in Section 4.

2. ITERATIVE MAP MODEL

To resolve some of the issues with an 'average' model, using separate GNLSEs for each component and region in the laser is common. Iteratively passing the pulse from one GNLSE to the next [7, 9, 10, 12]. This method allows for better encapsulation of specific dynamics introduced by each component. The main drawback of this method is the extreme computational expense since a nonlinear equation must be numerically solved for every segment for each of the hundreds of round trips in a given simulation. We can alleviate this computational expense by noticing each effect is localized to a corresponding component in the cavity: virtually all of the dispersion happens within the CFBG [31], the pulse is amplified only within the Er-doped fibre, *et cetera*. Therefore, we can drastically simplify each of the GNLSEs into a form we can solve analytically. Using analytic maps instead of numerically solving a GNLSE reduces the computational cost, while maintaining the benefit of reflecting the specific geometry of a component-wise simulation.

Iterative map methods have been used for optics since 1955 when Cutler [32] analyzed a microwave regenerative pulse generator. Siegman and Kuizenga [33–36] adapted Cutler's method for both AM and FM mode-locked lasers in 1969, and Martinez *et al.* [37, 38] incorporated the nonlinearity while modelling passively mode-locked lasers. A linear iterative method was used for dispersion-tuned actively mode-locked lasers recently by Burgoyne *et al.* [5]. Each of these models used a prescribed transfer function to describe the effect each component has on the pulse. While the transfer functions are chosen suitably to have the effect observed in the laboratory, the transfer functions are phenomenologically chosen, and not necessarily obtained directly from the underlying physics. Furthermore, these methods have not included the effect of every component, lacking the imperative interactions of dispersion, modulation, and nonlinearity—hindering their models to exhibit modulation instability.

We continue by deriving our own iterative map model by solving a reduced GNLSE for each component—except modulation, which we consider to be applied externally by an electro-optic modulator. Within the gain fibre, we assume all other effects are negligible. Any dispersion, for example, in the gain fibre pales in comparison to the dispersion introduced by the CFBG. Thus, we neglect the dispersion (as well as loss and nonlinearity by the same argument) in the gain fibre, allowing us to simplify Eq. (2) to

$$\frac{\partial A}{\partial z} = \frac{1}{2}g(A)A. \tag{3}$$

To proceed, we assume the gain has the form

$$g(A) = \frac{g_0}{1 + E/E_{\text{sat}}}, \tag{4}$$

where g_0 is a small signal gain, E is the energy of the pulse, defined as

$$E = \int_{-\infty}^{\infty} |A|^2 \, \mathrm{d}T, \tag{5}$$

and E_{sat} is the energy that the gain begins to saturate [6, 24, 27], which depends on the power of the pump laser. Thus, Eq. (3) becomes

$$\frac{\partial A}{\partial z} = \frac{g_0 A}{2(1 + E/E_{\text{sat}})}. \tag{6}$$

By assuming the energy entering the gain fibre is E_g and the energy after travelling through the gain fibre of length L_g is E_{out}, we find the energy after amplification is

$$E_{\text{out}} = E_{\text{sat}} W\left(\frac{E_g}{E_{\text{sat}}} \exp(E_g/E_{\text{sat}}) \exp(g_0 L_g)\right), \tag{7}$$

where W is the Lambert W function. Rewriting Eq. (7) in terms of the pulse gives

$$G(A) = \left(\frac{E_{\text{sat}}}{E_g} W\left(\frac{E_g}{E_{\text{sat}}} \exp(E_g/E_{\text{sat}}) \exp(g_0 L_g)\right)\right)^{1/2} A \tag{8}$$

for the amplification of the pulse after the Er-doped fibre.

Repeating the same procedure for the loss, dispersion, and nonlinearity yields

$$L(A) = (1 - R) \exp(-\alpha L_T) A, \tag{9}$$

$$D(A) = \mathcal{F}^{-1}\left\{\exp(i\omega^2 \beta_2 L_D/2)\mathcal{F}\{A\}\right\}, \tag{10}$$

$$F(A) = A \exp(i\gamma |A|^2 L_f), \tag{11}$$

where R is the reflectivity of the optical coupler, L_T is the total length of fibre in the cavity, L_D is the 'length' of the dispersive medium, L_f is the length of fibre between the amplifier and the optical coupler, and $\mathcal{F}$ denotes the Fourier transform.

Finally, we consider the modulation. Here, we assume the pulse is modulated by an electro-optic modulator. For simplicity, the form is taken as the Gaussian

$$M(A) = \exp(-T^2/2T_M^2) A, \tag{12}$$

where T_M is the characteristic width of the modulation. This assumption is not restrictive. Calcaterra and Boldt [39] have shown a sum of Gaussian functions can approximate any square integrable function. Therefore, our solution extends to any continuous, bounded modulation function. Additionally, using a saturable absorber in place of a modulator is common in practice. In this case, we can exchange Eq. (12) for [7, 9, 10, 12]

$$S(A) = \left(1 - \frac{q_0}{1 + |A|^2/P_{\text{sat}}}\right) A, \tag{13}$$

where q_0 is the modulation depth, $|A|^2$ is the instantaneous power of the pulse, and P_{sat} is the saturation power.

A. Non-Dimensionalization

Non-dimensionalization is a technique used in mathematical modelling to better understand the relative importance of different processes within a system. In essence, we scale all variables by typical values, based on the geometry and boundary conditions (see, for example, [40]). Doing so 'factors' the dimensional units out of the problem—leaving only dimensionless equations with dimensionless parameters. The relative magnitudes of the dimensionless parameters characterize the dominant dynamics—like how the Reynolds number describes fluid flow. Each process in the laser can be better understood by re-scaling the time, energy, and amplitude by the convenient scalings:

$$T = T_M \widetilde{T}, \qquad E = E_{\text{sat}} \widetilde{E}, \qquad A = \left(\frac{E_{\text{sat}}}{T_M}\right)^{1/2} \widetilde{A}. \tag{14}$$

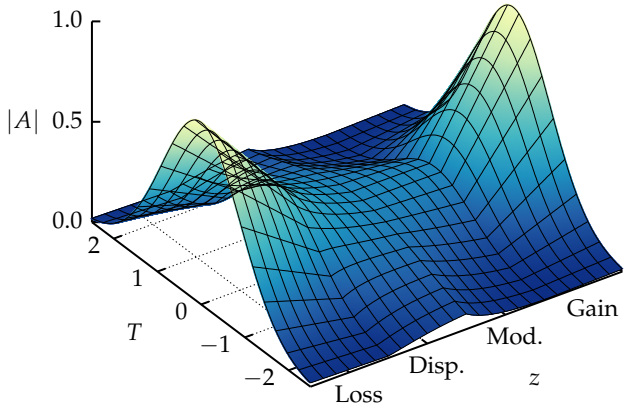

Fig. 2. Evolution of the envelope during one round trip of the cavity at equilibrium. The pulse decays because of the optical coupler, disperses because of the CFBG, is modulated by the modulator, and finally, is amplified by the gain fibre (the envelope is unaltered by the nonlinearity). Note, the z axis is not to scale.

Returning to the process maps Eq. (8)–Eq. (12), we find the non-dimensional mappings to be (after dropping the tildes)

$$\begin{aligned} &G(A) = \left(E_g^{-1} W\left(a E_g e^{E_g}\right)\right)^{1/2} A, \quad F(A) = \exp(ib|A|^2) A, \\ &D(A) = \mathcal{F}^{-1}\left\{\exp(is^2\omega^2)\mathcal{F}\{A\}\right\}, \quad L(A) = hA, \\ &M(A) = \exp(-T^2/2) A, \end{aligned} \tag{15}$$

with the four dimensionless parameters,

$$\begin{aligned} &a = \exp(g_0 L_g) \sim 8 \times 10^3, \quad h = (1 - R)\exp(-\alpha L_T) \sim 0.04, \\ &b = \gamma L_f \frac{E_{\text{sat}}}{T_M} \sim 1, \qquad s = \left(\frac{\beta_2 L_D}{2T_M^2}\right)^{1/2} \sim 0.2, \end{aligned} \tag{16}$$

as defined by the values in Table 1. Here, a is a measure of the strength of the gain fibre, h is the total loss due to absorption and the optical coupler, b is the frequency shift because of the Kerr nonlinearity, and s is the ratio of the effectiveness of the CFBG to the width of the pulse. Furthermore, in non-dimensional form, the modulation has no associated parameter, and each of the other processes in Eq. (15) have their own independent, non-dimensional parameter.

B. Combining the Component Maps

Now that we have the algebraic effect of each section of the cavity, we are ready to take the composition of the maps to give the effect of one round trip of the cavity. Unlike the models described in the beginning of this section, the permutation of our components is important as the maps in Eq. (15) do not necessarily commute with each other.

The geometry of a particular laser will dictate the order of the process maps. However, we assume the construction of the laser is as in Fig. 1, and provide the following justifications. The effect of the nonlinearity will be maximal after the pulse passes through the gain fibre—after the gain is where the pulse is most energetic. Thus, we take the nonlinearity component to follow the gain. Similarly, we want the loss component to directly follow the nonlinearity in an attempt to minimize the effect the nonlinearity has on the pulse. All that remains is the

Table 1. Range of parameter values (taken from [5, 18, 21, 29, 30]).

Parameter	Description	Value	Units
T_M	Characteristic modulation time	15–150	ps
$\beta_2 L_D$	Dispersion provided by the CFBG	10–2000	ps^2
γ	Kerr nonlinearity coefficient	0.001–0.01	$W^{-1}\,m^{-1}$
L_f	Length of fibre between gain and optical coupler	0.15–1	m
L_g	Length of the Er-doped gain fibre	2–3	m
α	Loss of fibre due to scattering and absorption	10^{-4}–0.3	m^{-1}
R	Reflectivity of optical coupler	0.1–0.9	–
E_{sat}	Saturation energy of Er-doped gain fibre	10^3–10^4	pJ
g_0	Small signal gain	1–10	m^{-1}
L_T	Total length of fibre in the cavity	10–100	m

dispersion and modulation components. For now, let us assume the CFBG precedes the modulator. Finally, we assume the loss component is our starting point since the loss corresponds to the optical coupler, and thus, allows us to more easily compare our results with experiments. More precisely, let

$$\mathcal{L}(A) = F(G(M(D(L(A))))) \tag{17}$$

denote one complete round trip of the cavity. Since a ring laser is cyclic in nature, we use the result of one round trip as the input pulse for the next round trip—restarting the process. We continually repeat this procedure until the envelope and chirp of the pulse reach equilibrium, or the pulse succumbs to modulation instability. The phase change is uninteresting to us, as Eq. (15) does not modify the phase in a meaningful way, and since the phase cannot easily be measured experimentally. An example of the evolution of the envelope during one round trip of the laser cavity can be found in Fig. 2.

3. RESULTS

We split the results into two subsections. In the following subsection we investigate the small nonlinearity limit, and in Section 3B we explore the full nonlinear model.

A. Linear Solution

By neglecting the effect of the nonlinearity, that is, taking $b = 0$, a solution can be found analytically. We proceed by assuming a fixed point solution will take the form of a linearly chirped Gaussian. The reasons for this assumption are that the solution to the models presented in [32, 33, 36–38] were Gaussian, the equilibrium shape will correlate to the modulation function, and a Gaussian is a fixed point of the Fourier transform. Furthermore, we choose a linearly chirped Gaussian because it resembles the envelope, and linear chirp expected from the literature [5, 26, 28, 30, 41].

Consider the pulse

$$A = \sqrt{P}\exp\left(-(1+iC)\frac{T^2}{2\sigma^2}\right)\exp(i\phi_0), \tag{18}$$

where P is the peak power, C is the chirp, σ^2 is the variance, and ϕ_0 is the phase (Fig. 3). By computing Eq. (18) after one round trip, and solving $\mathcal{L}(A) = Ae^{i\phi}$, a tedious manipulation yields the conditions

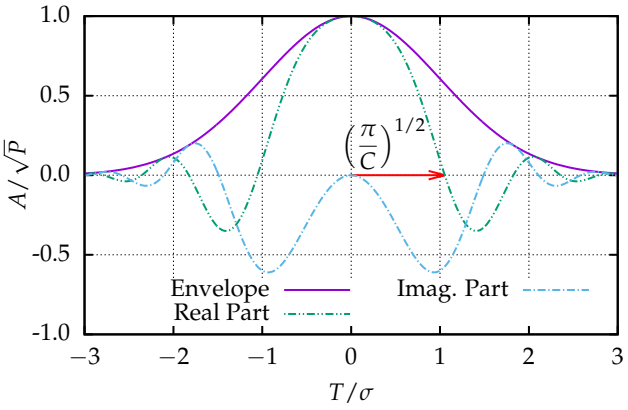

Fig. 3. Linearly chirped Gaussian pulse, Eq. (18) ($\phi_0 = 0$).

$$\frac{\sigma^4}{1-\sigma^2} = (\sigma^2 + 2Cs^2)^2 + 4s^4, \tag{19}$$

$$\frac{C}{1-\sigma^2} = C + 2\frac{s^2}{\sigma^2}(1+C^2), \tag{20}$$

$$1 = \frac{W(aE_g e^{E_g})}{E_g} h^2 (1-\sigma^2)^{1/2} \tag{21}$$

for Eq. (18) to be in equilibrium. Using Eq. (19) and Eq. (20) we are able to eliminate the chirp, and find the expression

$$\sigma^8 + 4s^4\sigma^6 - 20s^4\sigma^4 + 32s^4\sigma^2 - 16s^4 = 0, \tag{22}$$

which contains only σ^2 terms. Eq. (22) has an analytic solution, as is a quartic in σ^2, namely,

$$\sigma^2 = \sqrt{2}s\left(s^6 + 3s^2 + \sqrt{4+s^4}\left(1+s^4\right)\right)^{1/2} - s^4 - s^2\sqrt{4+s^4}. \tag{23}$$

Additionally, the chirp is

$$C = \frac{\sigma^4 - \left(\sigma^8 - 16s^4\left(1-\sigma^2\right)^2\right)^{1/2}}{4s^2(1-\sigma^2)}, \tag{24}$$

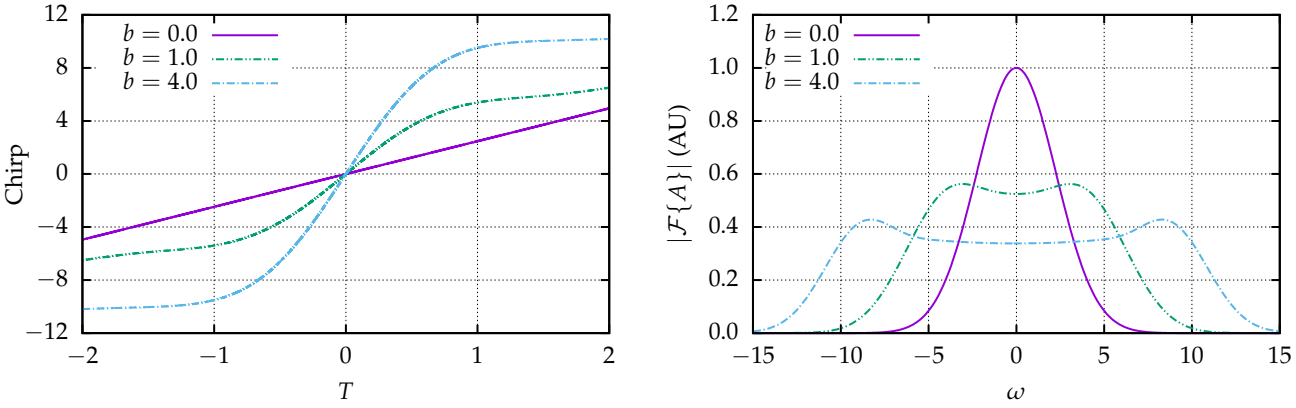

(a) Chirp.

(b) Fourier transform.

Fig. 4. Chirp and Fourier transform at equilibrium (after 500 round trips) initiated by Eq. (34) for three values of b, the nonlinearity parameter ($a = 8 \times 10^3$, $h = 0.04$, $s = 0.2$, and $E_0 = 0.1$).

in terms of s and σ^2. We can obtain the energy of the pulse entering the gain fibre, E_g, from Eq. (21), and thus, the equilibrium energy at the optical coupler. Doing so gives

$$E = \frac{\log\left(ah^2(1-\sigma^2)^{1/2}\right)}{1-h^2(1-\sigma^2)^{1/2}}. \tag{25}$$

By equating the energy of the pulse in Eq. (18) and Eq. (25), we find the peak power to be

$$P = \frac{\log\left(ah^2(1-\sigma^2)^{1/2}\right)}{\sqrt{\pi}\sigma\left(1-h^2(1-\sigma^2)^{1/2}\right)}. \tag{26}$$

The nature of Eq. (23)–Eq. (26) make the expressions difficult to work with. However, by asymptotically expanding Eq. (23)–Eq. (26) in terms of the dispersion parameter, s, we find the simpler relations

$$\sigma^2 \sim 2s(1-s) + \mathcal{O}\left(s^3\right), \tag{27}$$

$$C \sim 1 - s + \frac{1}{2}s^2 + \mathcal{O}\left(s^3\right), \tag{28}$$

$$E \sim \frac{\log(ah^2)}{1-h^2} - \frac{1}{1-h^2}\left(1 + \frac{h^2\log(ah^2)}{1-h^2}\right)s + \mathcal{O}\left(s^2\right), \tag{29}$$

$$P \sim \frac{\log(ah^2)}{\sqrt{2\pi}(1-h^2)}s^{-1/2} + \mathcal{O}\left(s^{1/2}\right), \tag{30}$$

in the case $s \to 0$. And,

$$\sigma^2 \sim 1 - \frac{1}{4}s^{-4} + \mathcal{O}\left(s^{-8}\right), \tag{31}$$

$$C \sim \frac{1}{2}s^{-2} + \mathcal{O}\left(s^{-6}\right), \tag{32}$$

in the case $s \to \infty$. We have no asymptotic expansion of the energy or peak power in the limit $s \to \infty$ since the pulse loses too much energy because of dispersion and modulation. The gain is not powerful enough to balance the energy lost. The argument of the logarithm in Eq. (25) gives us a condition for the pulse to be sustainable. Expanding the requirement $ah^2(1-\sigma^2)^{1/2} > 1$, from Eq. (25), using Eq. (31) (for a simple approximation), we find

$$s^* = \left(\frac{ah^2}{2}\right)^{1/2} \tag{33}$$

is the maximum value of s to facilitate a sustainable pulse.

Our linear model indeed exhibits a solution of the same form as previous linear models. However, by including the effect of the nonlinearity, we uncover the rich interplay between dispersion, modulation, and nonlinearity.

B. Nonlinear Solution and Instability

The nonlinear solution requires a numerical simulation, and so we must specify the input pulse—as in the laboratory. One of the common forms is a hyperbolic secant [8, 15, 16, 22], which we assume has the exact form

$$A_0 = \Gamma\,\mathrm{sech}(2T)e^{i\pi/4}. \tag{34}$$

Here, Γ is a normalizing factor chosen so the pulse has the initial energy E_0, which we take as $E_0 = 0.1$. Using Eq. (34) as a seed, we simulate the pulse travelling around the cavity using 2^{18} points, and a time span of 16.

In Fig. 4 we show the chirp and Fourier transform of the pulse Eq. (34) after reaching equilibrium for the nominal parameter values given in Eq. (16), and two additional b values. In the nonlinear case, we find the equilibrium pulse is no longer Gaussian—as evidenced by the Fourier transforms. Notice, in comparison to the linear case, the nonlinearity introduces higher frequency modes, giving a bi-modal distribution. Moreover, we find the pulse is linearly chirped near the peak, but, in the tails, $|T| \gtrsim 1$, the chirp begins to saturate—consistent with the experimental results [15, 17, 42]. As the nonlinearity parameter, b, increases, the chirp increases more sharply across the pulse, and saturates at a larger value. Also, the two peaks in the Fourier transform become more pronounced and further apart, and the Fourier transform of the pulse becomes more rectangular. However, after a critical point, SPM plays a more substantial role, leading to modulation instability.

Fig. 5 highlights the phenomenon of modulation instability. By decreasing the dispersion from Fig. 4, we find the pulse begins to 'breathe'. During the first two dozen round trips of the cavity the SPM compounds and becomes detrimental to the pulse. In turn, modulation instability is induced, and degrades the pulse, until the pulse is no longer stable or sustainable. On the other hand, having a more moderate value of b, the pulse is able to equilibrate even with a less favourable, random, initial pulse (Fig. 6), as in [10]. The pulse is able to shed the initial left

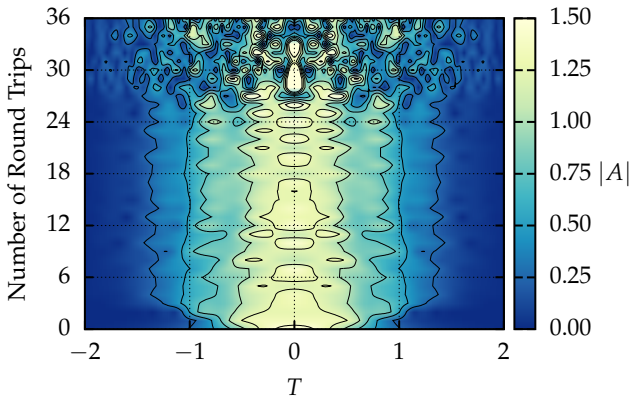

Fig. 5. Example of a pulse destabilizing from the initial pulse Eq. (34) ($a = 8 \times 10^3$, $h = 0.04$, $b = 1.6$, $s = 0.1$, and $E_0 = 0.1$).

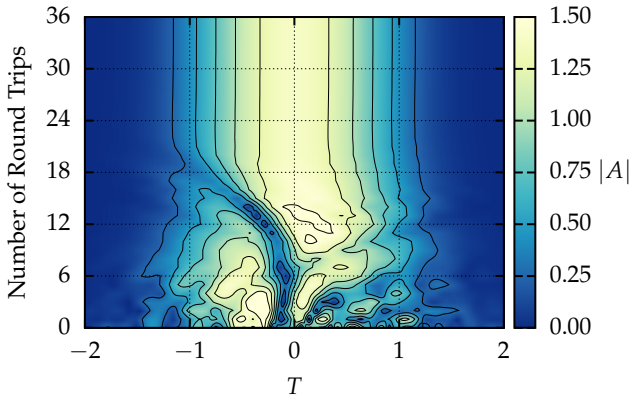

Fig. 6. Example of a pulse coming to equilibrium from noise ($a = 8 \times 10^3$, $h = 0.04$, $b = 1.0$, $s = 0.1$, and $E_0 = 0.1$).

lobe ($T \approx -1/2$) because of dispersion and modulation, and a central lobe ($T \approx 0$) forms, which is able to grow because of the gain medium. The central lobe then allows the pulse to come to equilibrium quickly. Furthermore, since the intensity of the initial pulse is small relative to the saturation energy, the effect of SPM is negligible during the first few round trips, allowing the laser to select preferable modes. The preferable modes then get amplified, stabilizing the pulse. Evidently, the initial shape of the pulse is much less important than the initial energy of the pulse, or the strength of the nonlinearity.

We now turn our attention to a more quantitative analysis, and characterize the stability of a laser by exploring the parameter space. We focus on the s–b plane in particular, since a and h affect only the amplitude of the pulse, whereas the interactions of dispersion and nonlinearity give rise to the instabilities. Additionally, as mentioned, a conservative initial energy will affect the dynamics much less than a more intense pulse since the nonlinearity will be negligible while initially coming to equilibrium. We examine the relative change in the pulse's envelope between consecutive round trips of the cavity to identify stability. We compute the error as

$$\Delta = \frac{\| |\mathcal{L}^n(A_0)| - |\mathcal{L}^{n-1}(A_0)| \|_2}{\|\mathcal{L}^{n-1}(A_0)\|_2}, \tag{35}$$

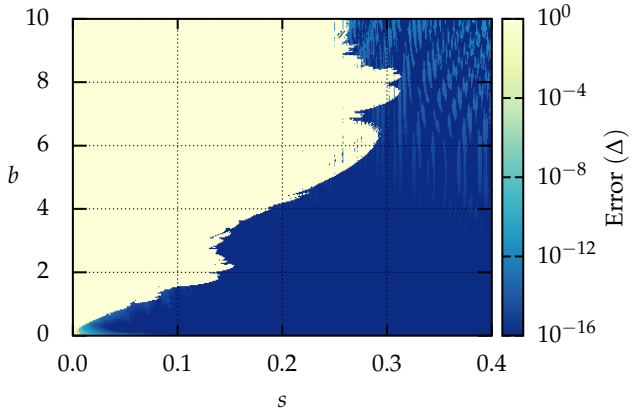

Fig. 7. Relative error of a pulse's envelope between round trips 499 and 500 ($a = 8 \times 10^3$, $h = 0.04$, and $E_0 = 0.1$).

where

$$\|f\|_2^2 := \int_{-\infty}^{\infty} |f|^2 \, \mathrm{d}T, \tag{36}$$

and we choose n to be sufficiently large to guarantee the pulse reaches equilibrium or deteriorates because of modulation instability—we use $n = 500$ in our experiments. We take the modulus of the pulse since we are interested in the evolution of only the envelope because of the auto-correlation methods used for experimental measurements. We plot the error in Fig. 7. Two distinct regions split the parameter space, divided by an incredibly sharp, and complicated boundary. In the upper-left region, the error is $\mathcal{O}(1)$; here, the nonlinearity is too strong, and the SPM induces modulation instability. In the lower-right region we find the opposite behaviour—the pulse reaches an equilibrium state and is stable. The increase in dispersion, coupled with modulation, allows the laser to balance the nonlinear effects. The error in this region is on the order of machine precision, suggesting the pulse has indeed reached to equilibrium.

Also of interest is the energy of the pulse at equilibrium, which we compute numerically by Eq. (5). Given our ordering of the components, we compute the energy of the pulse immediately before passing through the optical coupler. Thus, the energy of each pulse emitted by the laser is $(1 - h^2)E$, and $h^2 E$ remains in the cavity. We plot the energy in the s–b plane in Fig. 8. Unsurprisingly, we find the same sharp boundary as we saw in Fig. 7. In the unstable region (upper-left) the energy is small. The pulse is not able to foster prominent modes in this region and is unsustainable, thus, the intensity is low across the entire pulse. In the stable region (lower-right) we find the energy smoothly decays as both b and s increase, with the contours being hyperbolic-esque. As s increases, more energy is lost because of modulation since dispersion increases the length of the tails of the pulse. As b increases, our choice of modulation function helps suppress the additional frequencies generated by SPM, ensuring the pulse remains band-limited. We find a more energetic laser requires weaker dispersion, however, the nonlinearity must be correspondingly low, otherwise modulation instability will destroy the pulse. Moreover, the maximum energy, which occurs in the limit where both s and b go to zero, is 2.5487. With our choice of parameters, Eq. (29) predicts an equilibrium energy of 2.5535 at the origin, confirming the usefulness of the approximation.

Finally, we briefly investigate the affect the order of the components has on the dynamics. In Section 2B we justified the order

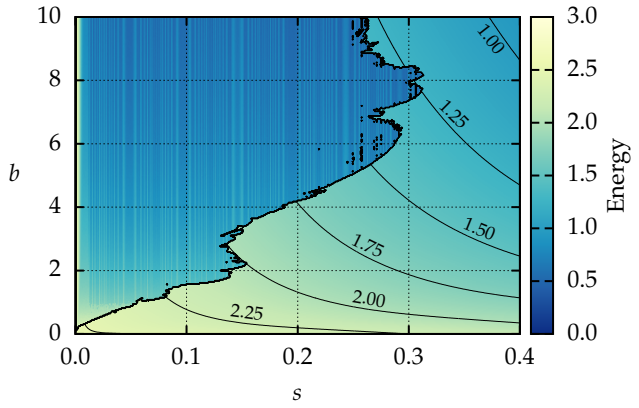

Fig. 8. Energy of the pulse after 500 round trips ($a = 8 \times 10^3$, $h = 0.04$, and $E_0 = 0.1$).

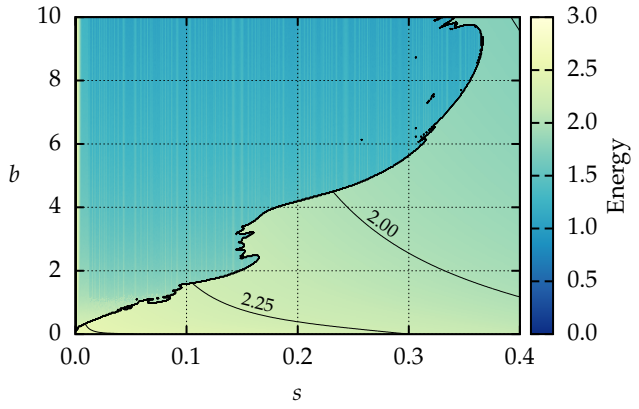

Fig. 9. Energy of the pulse after 500 round trips with dispersion and modulation swapped ($a = 8 \times 10^3$, $h = 0.04$, and $E_0 = 0.1$).

of the gain, nonlinearity, and loss, but, just assumed dispersion preceded modulation. Now, we consider the effect of swapping the dispersion and modulation components. The overall structure of the energy landscape (Fig. 9) is the same as in Fig. 8. In the previous case, with modulation following dispersion, more energy is removed from the pulse tails. Whereas, having modulation first, more energy remains in the cavity. The additional energy makes the laser more powerful than in the previous case, which in turn increases the size of the unstable region. Comparing with Fig. 8, the unstable upper-left region spreads farther rightward and upward, and the energy is larger in the stable region—especially away from the origin. Once again, the energy at the origin is 2.5487, as we are effectively removing the CFBG in the limit $s \to 0$.

4. CONCLUSION

Expanding upon the ideas originally proposed by Cutler [32], and Kuizenga and Siegman [33, 35, 36], we developed a nonlinear iterative map model for tuneable ring lasers. We recovered linearly chirped Gaussian solutions in the case of a Gaussian modulation function when omitting the nonlinearity. Moreover, the solution to the linear model extends to any modulation function using results of [39]. In contrast, with the inclusion of the nonlinearity, we were able to recover wave breaking and modulation instability, and found a sharp boundary of stability. These instabilities have been demonstrated in a laboratory setting [13, 15, 17, 18, 22], but, have proven difficult to predict with simple mathematical models [10]. We have shown a simple iterative map model is able to reproduce complicated instabilities arising naturally from the interplay between dispersion, modulation, and nonlinear effects. Our model easily adapts to specific laser geometries, and to more complicated models of individual components. For example, incorporating a frequency dependence in the gain function, or using a saturable absorber instead of a Gaussian modulator.

Analyzing the nonlinear model analytically using an asymptotic expansion for small values of the nonlinearity parameter, b, is of interest. Doing so will provide insight to how the nonlinearity impacts the linear solution to better understand the manifestation of wave breaking and modulation instability. Furthermore, a more detailed analysis of crossing the boundary between stability and instability may provide valuable insight for mechanisms that trigger the instability.

ACKNOWLEDGEMENT.

Portions of this work were presented at The V AMMCS International Conference in 2019, "A new method of modelling tuneable lasers with functional composition" [43]. BM acknowledges the support provided by the EPSRC Centre for Doctoral Training in Industrially Focused Mathematical Modelling (EP/L015803/1). The authors would like to thank C. Breward for critical reading of the manuscript.

DISCLOSURES.

The authors declare no conflicts of interest.

REFERENCES

1. H. Chung, W. Liu, Q. Cao, F. X. Kärtner, and G. Chang, "Er-fiber laser enabled, energy scalable femtosecond source tunable from 1.3 to 1.7 μm," Opt. Express **25**, 15760–15771 (2017).
2. C. S. Bohun, Y. Cher, L. J. Cummings, P. Howell, T. Mitre, L. Monasse, J. Mueller, and S. Rouillon, "Modelling and specifying dispersive laser cavities," in *Sixth Montréal Industrial Problem Solving Workshop*, (2015), pp. 11–25.
3. B. Burgoyne and A. Villeneuve, "Programmable lasers: Design and applications," in *Proc.SPIE*, vol. 7580 (2010), pp. 29–43.
4. S. Yamashita, Y. Nakazaki, R. Konishi, and O. Kusakari, "Wide and fast wavelength-swept fiber laser based on dispersion tuning for dynamic sensing," J. Sensors **2009**, 572835 (2009).
5. B. Burgoyne, A. Dupuis, and A. Villeneuve, "An experimentally validated discrete model for dispersion-tuned actively mode-locked lasers," IEEE J. Sel. Top. Quantum Electron. **20**, 390–398 (2014).
6. W. T. Silfvast, *Laser Fundamentals* (Cambridge University Press, 2004), 2nd ed.
7. B. Oktem, C. Ülgüdür, and F. O. Ilday, "Soliton–similariton fibre laser," Nat. Photonics **4**, 307–311 (2010).
8. S. Coen and M. Haelterman, "Modulational instability induced by cavity boundary conditions in a normally dispersive optical fiber," Phys. Rev. Lett. **79**, 4139–4142 (1997).
9. C. Lapre, C. Billet, F. Meng, P. Ryczkowski, T. Sylvestre, C. Finot, G. Genty, and J. M. Dudley, "Real-time characterization of spectral instabilities in a mode-locked fibre laser exhibiting soliton-similariton dynamics," Sci Rep **9**, 13950 (2019).
10. F. Meng, C. Lapre, C. Billet, G. Genty, and J. M. Dudley, "Instabilities in a dissipative soliton-similariton laser using a scalar iterative map," Opt. Lett. **45**, 1232–1235 (2020).
11. G. D. Shao, X. Hu, J. Guo, Y. F. Song, L. M. Zhao, D. Y. Shen, and D. Y. Tang, "Cavity-assisted modulation instability lasing of a fiber ring laser," Appl. Phys. B **125**, 5 (2019).

12. R. I. Woodward, "Dispersion engineering of mode-locked fibre lasers," J. Opt. **20**, 033002 (2018).
13. D. Anderson, M. Desaix, M. Lisak, and M. L. Quiroga-Teixeiro, "Wave breaking in nonlinear-optical fibers," J. Opt. Soc. Am. B **9**, 1358–1361 (1992).
14. J. E. Rothenberg and D. Grischkowsky, "Observation of the formation of an optical intensity shock and wave breaking in the nonlinear propagation of pulses in optical fibers," Phys. Rev. Lett. **62**, 531–534 (1989).
15. J. E. Rothenberg, "Femtosecond optical shocks and wave breaking in fiber propagation," J. Opt. Soc. Am. B **6**, 2392–2401 (1989).
16. W. J. Tomlinson, R. H. Stolen, and C. V. Shank, "Compression of optical pulses chirped by self-phase modulation in fibers," in *Conference on Lasers and Electro-Optics,* (Optical Society of America, 1984), pp. 139–149.
17. W. J. Tomlinson, R. H. Stolen, and A. M. Johnson, "Optical wave breaking of pulses in nonlinear optical fibers," Opt. Lett. **10**, 457–459 (1985).
18. G. Agrawal, *Nonlinear Fiber Optics* (Academic Press, 2013), 5th ed.
19. G. P. Agrawal, "Modulation instability induced by cross-phase modulation," Phys. Rev. Lett. **59**, 880–883 (1987).
20. M. Haelterman, S. Trillo, and S. Wabnitz, "Additive-modulation-instability ring laser in the normal dispersion regime of a fiber," Opt. Lett. **17**, 745–747 (1992).
21. B. Burgoyne (Personal communication, 2018). Halifax Biomedical Inc., 131 Shore Rd, Baddeck, NS B0E 1B0, Canada.
22. C. Finot, B. Kibler, L. Provost, and S. Wabnitz, "Beneficial impact of wave-breaking for coherent continuum formation in normally dispersive nonlinear fibers," J. Opt. Soc. Am. B **25**, 1938–1948 (2008).
23. J. Peng, H. Luo, and L. Zhan, "In-cavity soliton self-frequency shift ultrafast fiber lasers," Opt. Lett. **43**, 5913–5916 (2018).
24. O. V. Shtyrina, A. V. Ivanenko, I. A. Yarutkina, A. V. Kemmer, A. S. Skidin, S. M. Kobtsev, and M. P. Fedoruk, "Experimental measurement and analytical estimation of the signal gain in an Er-doped fiber," J. Opt. Soc. Am. B **34**, 227–231 (2017).
25. I. Yarutkina, O. Shtyrina, M. Fedoruk, and S. Turitsyn, "Numerical modeling of fiber lasers with long and ultra-long ring cavity," Opt. Express **21**, 12942–12950 (2013).
26. H. A. Haus, "A theory of forced mode locking," IEEE J. Quantum Electron. **11**, 323–330 (1975).
27. H. A. Haus, *Waves and Fields in Optoelectronics* (Prentice-Hall, Inc., 1984).
28. H. A. Haus, "Mode-locking of lasers," IEEE J. Sel. Top. Quantum Electron. **6**, 1173–1185 (2000).
29. K. Tamura and M. Nakazawa, "Dispersion-tuned harmonically mode-locked fiber ring laser for self-synchronization to an external clock," Opt. Lett. **21**, 1984–1986 (1996).
30. N. G. Usechak and G. P. Agrawal, "Rate-equation approach for frequency-modulation mode locking using the moment method," J. Opt. Soc. Am. B **22**, 2570–2580 (2005).
31. G. Agrawal, *Fiber-Optic Communication Systems* (John Wiley & Sons, Inc., 2002), 3rd ed.
32. C. C. Cutler, "The regenerative pulse generator," in *Proceedings of the IRE,* (IEEE, 1955), pp. 140–148.
33. D. J. Kuizenga and A. E. Siegman, "FM and AM mode locking of the homogeneous laser - Part I: Theory," IEEE J. Quantum Electron. **6**, 694–708 (1970).
34. D. J. Kuizenga and A. E. Siegman, "FM and AM mode locking of the homogeneous laser - Part II: Experimental results in a Nd:YAG laser with internal FM modulation," IEEE J. Quantum Electron. **6**, 709–715 (1970).
35. D. J. Kuizenga and A. E. Siegman, "FM-laser operation of the Nd:YAG laser," IEEE J. Quantum Electron. **6**, 673–677 (1970).
36. A. E. Siegman and D. J. Kuizenga, "Simple analytic expressions for AM and FM modelocked pulses in homogenous lasers," Appl. Phys. Lett. pp. 181–182 (1969).
37. O. E. Martinez, R. L. Fork, and J. P. Gordon, "Theory of passively mode-locked lasers including self-phase modulation and group-velocity dispersion," Opt. Lett. **9**, 156–158 (1984).
38. O. E. Martinez, R. L. Fork, and J. P. Gordon, "Theory of passively mode-locked lasers for the case of a nonlinear complex-propagation coefficient," J. Opt. Soc. Am. B **2**, 753–760 (1985).
39. C. Calcaterra and A. Boldt, "Approximating with gaussians," ArXiv (2008). ArXiv:0805.3795.
40. S. Howison, *Practical Applied Mathematics: Modelling, Analysis, Approximation*, Cambridge Texts in Applied Mathematics (Cambridge University Press, 2005).
41. H. A. Haus, "Theory of soliton stability in asynchronous modelocking," J. Light. Technol. **14**, 622–627 (1996).
42. Q. Chen, N. Lu, and F. Jiang, "Characterization of the dispersion of chirped fiber Bragg grating through fourier transform spectrometry method," in *Proc.SPIE,* vol. 6837 (2008), pp. 216–223.
43. B. Metherall and C. S. Bohun, "A new method of modelling tuneable lasers with functional composition," in *The V AMMCS International Conference,* (To appear).